J Solid State Electrochem (2010) 14:313–321
DOI 10.1007/s10008-009-0855-9

ORIGINAL PAPER

Diamond/porous titanium three-dimensional hybrid electrodes

N. A. Braga · C. A. A. Cairo · J. T. Matsushima · M. R. Baldan · N. G. Ferreira

Received: 6 January 2009 / Revised: 3 April 2009 / Accepted: 22 April 2009 / Published online: 9 May 2009

Abstract Hybrid three-dimensional electrodes produced from microcrystalline boron-doped diamond (BDD) and/or nanocrystalline diamond films were grown on porous titanium (Ti) substrate by hot filament chemical vapor deposition (HFCVD) technique. Powder metallurgy technique was used to obtain the Ti substrates provided by interconnected and open pores among its volume. Diamond growth parameters were optimized in order to provide the entire substrate surface covering including the deeper surfaces, pore bottoms, and walls. The morphology and structure of these electrodes were studied by scanning electron microscopy (SEM) and visible Raman spectroscopy techniques, respectively. Electrochemical response was characterized by cyclic voltammetry measurements. Results showed a wide working potential window and low background current characteristic of the diamond electrodes. The kinetic parameters also pointed out to a quasi-reversible behavior for these hybrid three-dimensional diamond/Ti electrodes.

Keywords Porous titanium · Diamond · Electrodes · Three-dimensional porosity

N. A. Braga · J. T. Matsushima (✉) · M. R. Baldan · N. G. Ferreira
Instituto Nacional de Pesquisas Espaciais, INPE,
12245-970 São José dos Campos, São Paulo, Brazil
e-mail: jtmatsushima@yahoo.com.br

C. A. A. Cairo
Comando-Geral de Tecnologia Aeroespacial, CTA,
12228-904 São José dos Campos, São Paulo, Brazil

Introduction

Recent technological breakthroughs and the desire for new functions generate an enormous demand for novel materials. In this sense, the possibility to combine the materials as inorganic/organic, for example, gives rise to novel insights into hybrid materials that leads to new properties in such materials. One example is the manufacturing of boron-doped diamond (BDD) films on metallic substrates. Concerning this subject, the engineering of nanometer and/or micrometer-sized organization of materials like metallic titanium and non-metallic diamond gives rise to a kind of interesting electrochemical devices.

As far as characteristics features of Ti are concerned, recent work by ourselves [1, 2] and others [3] have shown that, during the deposition process of diamond by hot filament chemical vapor deposition (HFCVD), two crystalline phases are generated at the film/substrate interface: TiC and TiH_2. The formation of these phases presents a strong influence on the properties of diamond coating. In our previous paper, we obtained diamond film by means of HFCVD method. In general, X-ray diffraction analytical techniques and Raman spectroscopy were used to investigate the influence of deposition temperature as well as the influence of the argon concentration on the diamond morphology and quality. Knowledge of the temperature variation and also the influence of Ar concentration allow us to optimize the best parameters to grow BDD/Ti and nanocrystalline diamond (NCD)/Ti with the objective to use as electrodes.

Polycrystalline conductive diamond films are excellent candidates to work as electrode materials for showing a wide potential window, high corrosion resistance and also mechanical stability when compared with other electrode

materials commonly used, such as glass carbon, graphite, and platinum [4, 5]. Pleskov et al. [6] were the first ones to study the electrochemical and photoelectrochemical behavior of the diamond electrodes. From this work, many studies have been carried out with these electrodes with the objective of characterizing it electrochemically, pointing out its wide range of application [7–10].

Electrochemical experiments for the verification of the potential window [5, 11] and resistance to the corrosion in extremely aggressive environments have also been carried out and compared with other usual carbon electrodes [12–14]. The great advantage of the diamond electrode is its potential window of approximately 3.0 V, greater than those usually used in electrochemical analyses. Therefore, it allows the detection of redox reactions that would be out of the range of the working potential of the conventional electrodes.

To characterize the diamond electrode, some studies of electron transfer kinetic in the interface of the semiconductor/electrolyte, reversibility of the redox reactions [5, 15], and superficial treatments have been carried out in order to evaluate its influence in the electrochemical properties of the doped diamond electrodes [16–18]. Some works were carried out with the purpose to evaluate the sensitivity, precision, stability, and resolution and have presented the potentiality of the diamond as electrochemical sensors [19–22]. The use of these electrodes made possible the detection of diverse types of chemicals substances, such as uric acid [19], polyamines [20], Pb traces in water [21], and among others. In particular, porous electrodes have attracted special attention due to its applications in electroanalysis, electrocatalysis, batteries, supercapacitors, and fuel cells [23–26].

The diamond deposition on Ti substrates with high and interconnected porosity appears as a novel and unexplored area. Such substrates may be obtained by powder metallurgy process by varying the porosity level, porosity distribution, pore size, and shape and, as consequence, their mechanical properties [27]. Several factors are found to limit the use of diamond deposited on Ti substrates. Among the difficulties, the poor adhesion, due to diamond/Ti mismatch and the difference of the thermal expansion coefficients between diamond and Ti, may be highlighted. Besides, the rapid in-diffusion of light elements forming non-diamond species promotes the hydrides formation, which cause a degradation of the mechanical properties of the Ti substrates [28, 29]. However, an interfacial TiC layer may minimize the residual thermal stress between substrate and the diamond film. The great challenge, in this case, is to control the growth experimental conditions to understand the effect of the hydrogenation and the role of the Ti hydride formation in the mechanism of diamond chemical vapor deposition on these substrates.

There are few works in the current literature that discuss the preparation and characterization of diamond electrodes deposited on Ti substrates [30–32], and as far as we know, there are no works in the literature describing hybrid three-dimensional porous BDD/Ti and NCD/Ti electrodes and their electrochemical response. Such electrodes can link the structural advantages of the metallic Ti structure, with the advantages to the slightness of the structures contending porosity introduced in the bulk material, adding yet to the excellent structural, chemical properties and stability of the diamond.

This work presents the aspects related to the formation of two new hybrid diamond electrodes obtained by HFCVD technique. One of them is composed by BDD film deposited on a three-dimensional titanium matrix (BDD/Ti) and the other one formed by a NCD film deposited on such substrate (NCD/Ti). The morphologic and structural characterization of these two hybrid electrodes is performed as well as their electrochemical performance, which was evaluated by cyclic voltammetry measurement. The electron transfer kinetic using $Fe(CN)_6^{4-/3-}$ redox system was also evaluated.

Experimental

Powder metallurgy was used to prepare Ti substrate with desired three-dimensional porosity from pure Ti powder by pre-form sintering. The details of this process were recently published in the previous paper [33]. One of these hybrid electrodes called BDD/Ti was obtained by a BDD film growth on a three-dimensional porous Ti substrate by HFCVD technique. The conditions used for the BDD deposition on such substrate were the following: temperature in the 600–620 °C range, filaments distance of 7 mm, total pressure inside the reactor chamber of the 20 Torr, and deposition time of 8 h. BDD films were obtained from a 1.0% vol. H_2/CH_4 mixture, and boron was added from an additional H_2 source forced to pass through a bubbler containing B_2O_3 dissolved in CH_3OH. For all experiments, H_2 and $B_2O_3/CH_3OH/H_2$ flows were controlled in order to obtain the desired B/C ratio in CH_3OH. This film presents a doping level of approximately 10^{18} boron atoms per cubic meter, previously estimated from Mott Schttky plot for samples grown with similar boron content [34].

The second electrode was obtained by NCD deposition (without doping) on the same type of substrate and called NCD/Ti. The experimental growth parameters were substrate temperature of 600 °C, filament distance of 6 mm, total gas pressure inside the reactor of 50 Torr, deposition time of 8 h, and gas concentrations of 1.5, 8.5, and 90% vol. of CH_4, H_2, and Ar, respectively. Top view scanning

electron microscopy (SEM) images of BDD and NCD films were obtained from a Jeol equipment JSM-5310. The quality of BDD and NCD films was analyzed from Micro-Raman spectra recorded by a Renishaw microscope system 2000 in backscattering configuration.

The electrochemical measurements were carried out using a three-electrode electrochemical cell. BDD/Ti or NCD/Ti films were used as working electrode. Platinum semi-circular was used as counter-electrode and a commercial Ag/AgCl electrode (3.0 mol L^{-1} KCl solutions) served as the reference. The working electrodes were not submitted to surface pretreatment before electrochemical measurements. All electrochemical measurements were carried out using a potentiostat/galvanostat AUTOLAB model PGSTAT 302. Cyclic voltammetry measurements were used for the electrochemical characterization with KCl solution (working potential window) and $Fe(CN)_6^{4-/3-}$ redox system for the electron transfer kinetic study of BDD/Ti and NCD/Ti electrodes. Before each measurement, the solution was previously deoxygenated with gaseous N_2 for at least 20 min. The experiment was carried at room temperature.

Results and discussions

The present discussion will be focused on the aspects related with the structure and morphology of the electrodes manufactured on this work as well as their contribution for the electrochemical conductivity of them. The aspects related to the substrate preparation were previously published [33]. The top view SEM images of the diamond films deposited on three-dimensional Ti substrates are represented in Fig. 1a–d and its insets. The Fig. 1a and c corresponds to the BDD/Ti, whereas Figs. 1b and d corresponds to the NCD/Ti electrodes surface morphologies. In order to visualize the morphologic changes and to confirm the diamond film coating through the entire substrate, the Fig. 1a inset shows the three-dimensional Ti substrate without the diamond film. The Fig. 1c shows surface morphology of the same BDD/Ti electrode in higher magnification. This image refers to the top surfaces of such electrode. We define top surfaces (planes or declivity) as the diamond surface area nearest the filament during the deposition process and deep surface areas (planes, declivity, pores, and walls) to regions located below of the top surfaces. Figure 1c inset corresponds to a deep surface area of the BDD/Ti electrode. In the same way, the Fig. 1b is associated to the general view of the NCD/Ti electrode surface morphology, and Fig. 1d and its inset correspond to the NCD/Ti electrode top and deep surfaces morphology, respectively.

The images in Fig. 1 confirm that the films grown on the three-dimensional Ti substrate did not present fissures or delaminations. Besides, the substrate was totally covered, including its borders (Figs. 1a, b) keeping its original feature. This aspect is also observed in the deeper surfaces of the samples, which can be seen in the insets of Figs. 1c and d. These insets illustrate the images obtained from diamond film coating on the substrate surfaces, localized into the pores or deeper surfaces of the BDD/Ti (Fig. 1c inset) and NCD/Ti (Fig. 1d inset), leading to a three-dimensional porous diamond/Ti hybrid material. In order to grow diamond films in three-dimensional Ti matrices different contributions must be considered: (1) the amount of atomic hydrogen available at different depths (top and deeper surfaces) and (2) the high thermal gradient established between these different depths, which influence the reactions on the surface and the variation of the localized thermal and/or intrinsic stresses [2]. Besides, the control of the substrate porosity also presents an important role in the process and contributes to the better adhesion of the film and, consequently, to the film stress relief.

The gaseous composition does not only influence the growth and nucleation rate but also the morphology of the resultant diamond film [35, 36]. These aspects may be observed in BDD and NCD films in two different ways. First, by comparing the films obtained at most external regions (top surfaces) of the BDD/Ti and NCD/Ti electrodes, the introduction of the argon (for NCD/Ti electrode manufacturing) and, consequently, the decrease in the hydrogen amount changes the morphology from a well-faceted grain in BDD film (Fig. 1c) to a smoothness ball-like structure, composed by agglomerates of small grains (Fig. 1d), frequently called cauliflower-like structure, also typical of NCD films. Secondly, by comparing the same electrode in two different regions (top and deep surface), the influence of the gaseous composition was different for the diamond growth on the top of the BDD/Ti sample (Fig. 1c), where the dominant structure observed is the typical microcrystalline diamond, with average size of 1 μm, characteristic of high growth and nucleation rate of the film. In its more internal regions, which are evident in the images of the Fig. 1c inset, the dominant aspect of the grain size reduction and cauliflower formation are observed.

The literature attributes the cauliflower diamond formation to the process of nucleation and renucleation [37, 38]. This process strongly affects the grain size and film agglomerate formation. Whereas BDD/Ti electrode is concerned on the atmosphere formation composed essentially by a high amount of H_2 and CH_4, which contributes for well-faceted microcrystalline diamond grains with crystallographic orientation varying between <111> and <200> (Fig. 1c), the poor H_2 environment for the NCD/Ti electrode formation contributed for nanocrystalline diamond grains (Fig. 1d). In this sense, the cauliflower

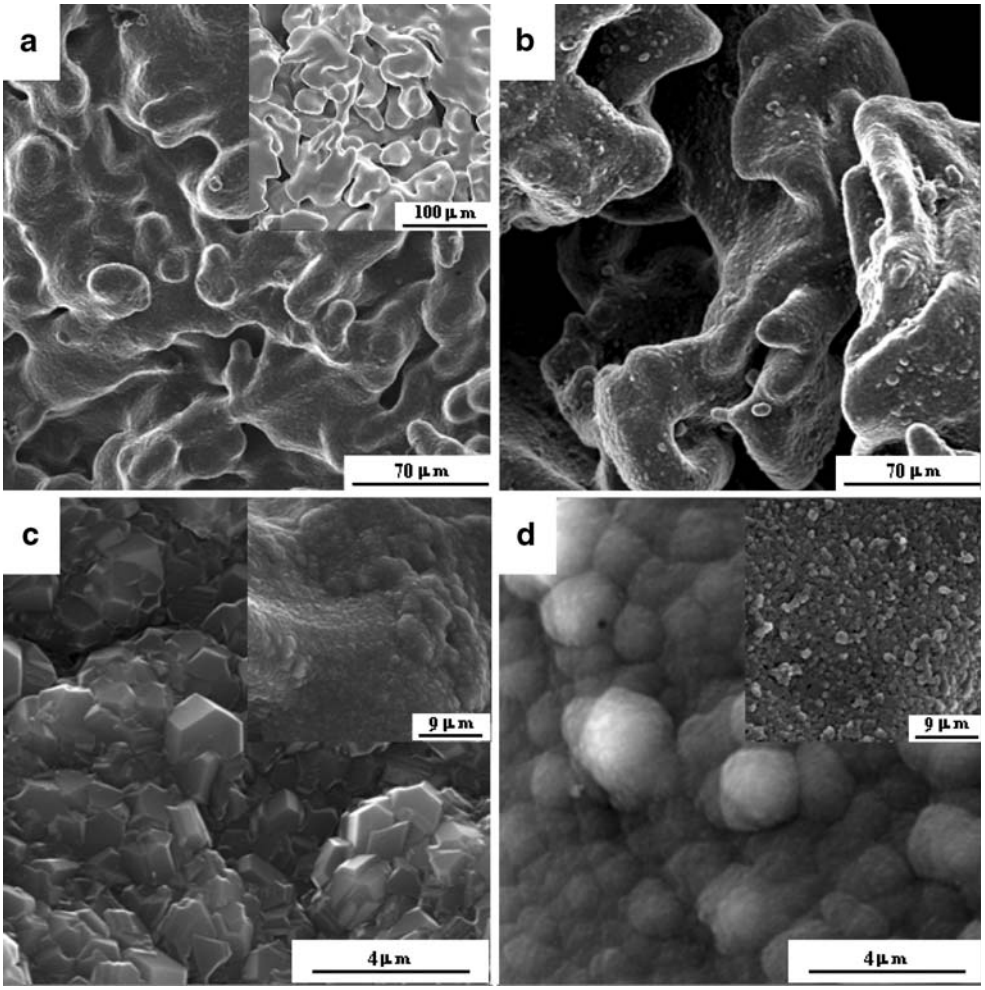

Fig. 1 SEM images of the three-dimensional diamond/Ti hybrid electrodes: **a** general view of the BDD/Ti electrode surface morphology; **a**, *inset* three-dimensional Ti substrate without the diamond film; **b** general view of the NCD/Ti electrode surface morphology; **c** BDD/Ti electrode top surfaces morphology; **c**, *inset* BDD/Ti electrode deeper surfaces morphology; **d** NCD/Ti electrode top surfaces morphology; **d**, *inset* NCD/Ti electrode deeper surfaces morphology

structure may also be rationalized in terms of the atomic H viability. The role of the atomic H is to react with the hydrocarbons from the gas phase, transforming them into species that could contribute significantly to surface growth. Besides, the abstraction of surface H atoms by atomic H from the gas phase to form surface sites and the subsequent reactions with C_1 species determine the probability of nucleation/renucleation and hence the morphology of the film [39]. The effect of H reduction away from the filaments (hole regions or deeper surfaces of the sample), due to the faster recombination on the surfaces, and the decrease in pertinent growth species (C_1 and C_2), due to the shorter mean free path, justify the changes in the morphology from the most external to the most internal regions. However, to understand the nucleation and the renucleation mechanism, at great depths, requires additional study.

With the purpose of analyzing the composition and the quality of the diamond films of the BDD/Ti and NCD/Ti electrodes, the Raman spectra of these films were registered and are presented in Fig. 2. The presence of a Raman peak in the region of 1,332 cm^{-1} was verified, which corresponds to the vibration of a diamond first-class phonon [40]. This peak is the Raman signature for the diamond and is more apparent, as expected, for BDD/Ti film. Around 1,350 cm^{-1}, the D band appears for both films due to disordered structures and, around 1,590 cm^{-1},

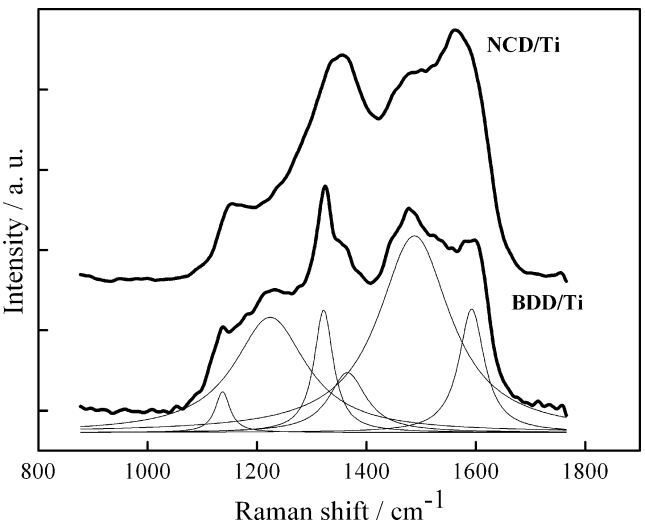

Fig. 2 Raman spectra of BDD/Ti electrode and NCD/Ti electrode

appears a G peak corresponding to the graphite [41]. The presence of a band around 1,200 cm^{-1} is distinguished in the Raman spectrum of the BDD/Ti film and is attributed to the relaxation of the selection rule $k=0$ of the Raman scattering due to presence of one high concentration of B in the crystalline net of diamond [43, 44]. This band confirms the doping of the diamond film. An important aspect to be detached in the Raman spectra of both BDD/Ti and NCD/Ti films is the presence of the peaks around 1,140 and 1,470 cm^{-1}, which has been attributed [42, 45, 46] to the trans-polyacetylene presence that is a polymeric compound formed in the grain boundaries of diamond films with nanometer dimensions.

Particularly, the spectra presented in Fig. 2 for the BDD/Ti film is associated to the diamond film obtained using a standard composition for the microcrystalline diamond deposition (but with boron as doping agent). Despite this condition, it is also observed that the presence of the trans-polyacetylene peak is associated to NCD formation. This formation of NCD can be attributed to the poor atomic hydrogen concentration in the Ti matrix deeper surfaces, concerning the most internal or holes of the substrate, leading to a reduction in the growth rate of the diamond grain. Then, the contribution of the diamond layers in these more internal surfaces, with smaller grains than those observed in the top film surface, becomes representative in the spectrum of the BDD/Ti film, generating the observed NCD contribution.

Figure 3 presents the cyclic voltammetric curves for BDD/Ti, NCD/Ti, and platinum electrodes in 1.0 mol L^{-1} KCl solution. The voltammetric behavior indicated that BDD/Ti and NCD/Ti electrodes present a working potential window of approximately 3.3 V versus Ag/AgCl. This value is similar to that already described in the literature for BDD and NCD films deposited on silicon [47, 48] but much broader when compared with others commonly used as electrode materials, such as platinum (~2.0 V, see Fig. 3), vitreous carbon (~2.5 V), and graphite (~2.0 V) electrodes [49]. The wide working potential range (up to 3.0 V) presented by BDD/Ti and NCD/Ti electrodes, which defines the higher cathodic and anodic limits for water decomposition reaction (reduction and oxidation), is one of the main parameters for the detection of many electroactives species in aqueous electrolytes, without the interference of the water reduction and oxidation reactions. For both electrodes, the onset of hydrogen evolution due to water reduction is verified to begin at −1.6 V, whereas the onset of oxygen evolution due water oxidation begins at 1.7 V. It is also observed that the contribution of the capacitive background current is involved in the electric double-layer charging, which is associated to the surface area exposed to the solution and also to the amount of sp^2-bonded carbon impurities exposed at the grain boundaries. According to Show et al. [50], this carbon is a source of π states that contribute to the density of electronic states in the material, increasing the capacitive component of the background current. The amount of sp^2-bonded carbon impurities present in the BDD/Ti and NCD/Ti electrodes was confirmed by Raman spectroscopy, and the results were shown in Fig. 2. When compared with platinum electrode (see Fig. 3), these electrodes represent low capacitive background current, justifying the excellent stability suited for current based electrochemical measurements. In particular, this characteristic associated to higher anodic limit makes them as excellent anode materials to be used in electro-oxidation of organic species [51]. In this way, these electrodes have been used in wastewater treatments promoting the combustion of organic pollutants occurring at high current efficiency [52].

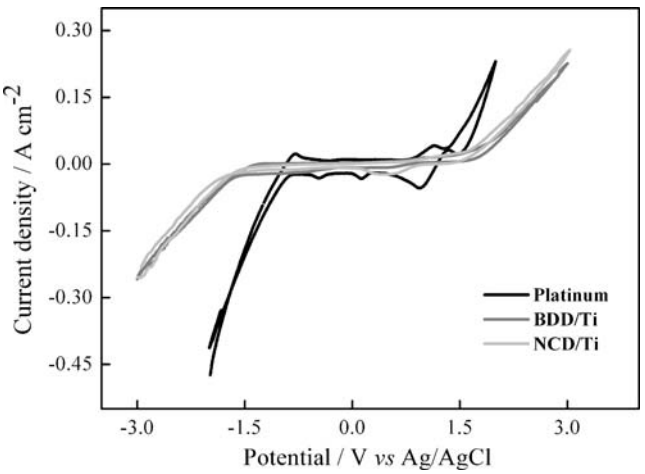

Fig. 3 Cyclic voltammograms for BDD/Ti, NCD/Ti, and Pt electrodes in 1.0 mol L^{-1} KCl solution, $v=50$ mV s^{-1}

The characterization of the working potential window and capacitive currents from cyclic voltammograms is presented in Fig. 3, showing clearly that the properties of diamond films deposited on porous Ti substrate have similar electrochemical properties when compared to the diamond films deposited on silicon substrate. On the other hand, they presented better electrochemical properties than the platinum electrode.

Besides the analysis with respect to working potential window and the background currents for electric double-layer charging, it is also common to evaluate the electrode kinetics for the occurrence of redox reactions through the electrode/electrolyte interface. The $Fe(CN)_6^{4-/3-}$ redox couple is one of the most used for the characterization of diamond electrodes, since the electrode reaction kinetics for this redox couple is sensitive to the presence of exposed edge plane on sp^2-bonded carbon in microcrys-

talline BDD and nanocrystalline diamond films. Using this redox couple, kinetic parameters, such as peak potential separation (ΔE_p) and peak current (I_p) versus square root scan rate ($v^{1/2}$) obtained from cyclic voltammograms, can easily be evaluated.

Figures 4 and 5 show cyclic voltammograms for BBD/Ti and NCD/Ti electrodes, respectively, obtained at different scan rates in 1.0 mmol L^{-1} $Fe(CN)_6^{4-/3-}$ +1.0 mol L^{-1} KCl solution. The voltammetric response of $Fe(CN)_6^{4-/3-}$ redox couple for the two electrodes is quite similar. However, a shift in the of anodic and cathodic peak potential as function of the scan rate was observed. Similar observations have been reported for as-grown BDD electrodes with a sufficiently high boron doping level [53, 54]. For both electrodes, the peaks are not well defined. In particular, in the BDD/Ti electrode (Fig. 4), in the anodic sweep after the peak, the current does not decay for a characteristic constant value of the diffusion limit current. This behavior may be explained, assuming that the $Fe(CN)_6^{4-/3-}$ diffusion from the top of electrode surface is different compared to that at deeper electrode regions. This behavior may be associated to the different porosity and surface roughness in the BDD/Ti electrode that leads to a concentration gradient of species present in the solution. In this sense, the area available to the electrochemical process decreases, principally at high scan rates. This same behavior was not observed in the NCD/Ti electrode (Fig. 5). The NCD/Ti film showed to be more homogeneous without considerable variation on its morphology. In addition, for the NCD/Ti electrode, during the cathodic sweep, a current diffusion limit smaller than that for the beginning of the sweep can be seen. For this case, the difference may be associated to the background current due to the large amount of sp^2 carbon impurities exposed at the grain boundaries. Unfortunately, for diamond films grown on Ti substrate, there is not a conclusive evidence to explain the peak features presented during the electrode kinetic studies.

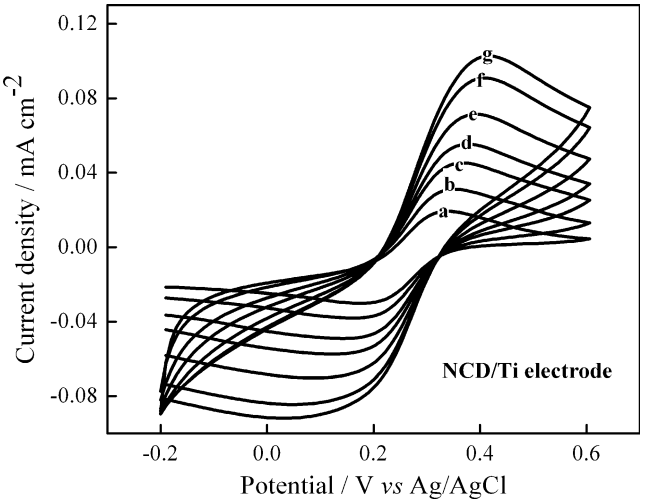

Fig. 5 Cyclic voltammograms for NCD/Ti electrode obtained at different scan rate: **a** 5, **b** 10, **c** 20, **d** 40, **e** 60, **f** 80, and **g** 100 mV s^{-1} in 1.0 mmol L^{-1} $Fe(CN)_6^{4-/3-}$ +1.0 mol L^{-1} KCl solution

Figure 6 presents plots of ΔE_p versus scan rate for the BDD/Ti and NCD/Ti electrodes obtained in 1.0 mmol L^{-1} $Fe(CN)_6^{4-/3-}$ +1.0 mol L^{-1} KCl solution. For both electrodes, ΔE_p increases with the increase of scan rate, but the ΔE_p values obtained for BDD/Ti electrode were smaller when compared to those for NCD/Ti electrode. At low scan rate, the ΔE_p tends to approach 60 mV for the BDD/Ti

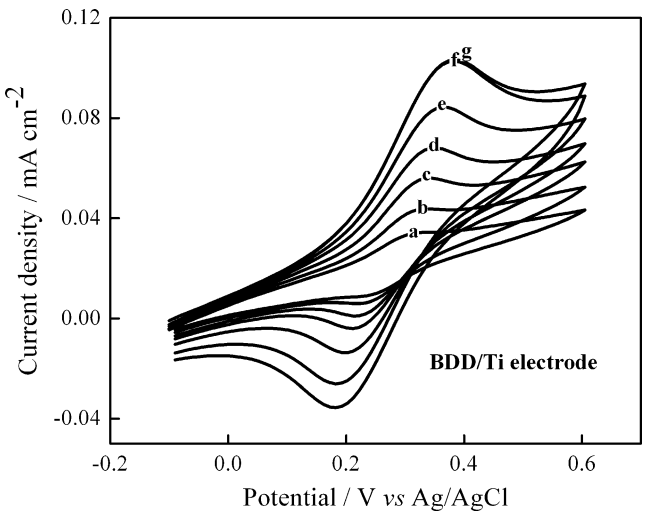

Fig. 4 Cyclic voltammograms for BBD/Ti electrode obtained at different scan rate: **a** 5, **b** 10, **c** 20, **d** 40, **e** 60, **f** 80, and **g** 100 mV s^{-1} in 1.0 mmol L^{-1} $Fe(CN)_6^{4-/3-}$ +1.0 mol L^{-1} KCl solution

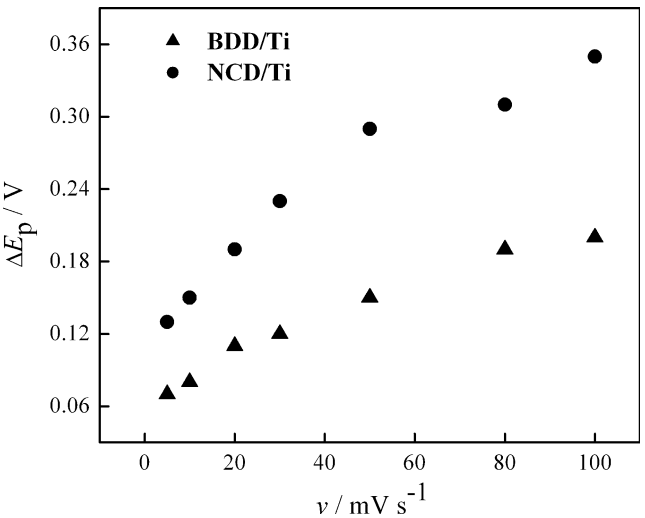

Fig. 6 Plots of ΔE_p versus scan rate for the BDD/Ti and NCD/Ti electrodes obtained in 1.0 mmol L^{-1} $Fe(CN)_6^{4-/3-}$ +1.0 mol L^{-1} KCl solution

electrode, whereas that of the NCD/Ti electrode tends to approach 120 mV. According to the criteria used for testing the electron transfer reaction kinetic [55], the ΔE_p of 59/n mV (where n is the number of electrons involved in the reaction and n=1 for $Fe(CN)_6^{4-/3-}$ redox couple) is one of the indications of a quasi-reversible system. In this way, the BDD/Ti electrode presents a quasi-reversible at behavior low scan rates. In general, the difference with regard to ΔE_p might be associated to surface microstructure, the presence of surface carbon–oxygen functionalities as well as the surface cleanliness of sp^2-bonded carbon electrodes [56]. In the case of the NCD/Ti electrode, the ΔE_p increase may be attributed to the presence of a high amount of the sp^2-bonded carbon when compared with the BBD/Ti electrode, as observed in the Raman spectra shown in Fig. 2. This high amount of sp^2 site is responsible for the formation of a large content of oxygen terminated in the surface of NCD/Ti electrode, which has the function to block active sites to occur in redox reactions and, consequently, to promote a decrease of the electron transfer kinetic for the BDD/Ti electrode. Granger et al. [53] showed that surface carbon–oxygen functionalities on microcrystalline diamond significantly influence ΔE_p with increasing oxygen content, causing an increase in the peak potential separation. A similar effect was also observed by Fujishima and co-works [54].

Another criterion to evaluate the electrode kinetic is to analyze the behavior of I_p as a function of $v^{1/2}$. Figure 7 presents plots of I_p versus $v^{1/2}$ for the BDD/Ti and NCD/Ti electrodes obtained in 1.0 mmol L^{-1} $Fe(CN)_6^{4-/3-}$ + 1.0 mol L^{-1} KCl solution. For the NCD/Ti electrode, it can be seen that I_p varies linearly with $v^{1/2}$ with a near zero y-axis intercept, which is an indication of reactions limited by semi-infinite linear diffusion of reactants to the electrode surface. Despite of the small deviation of the zero y-axis

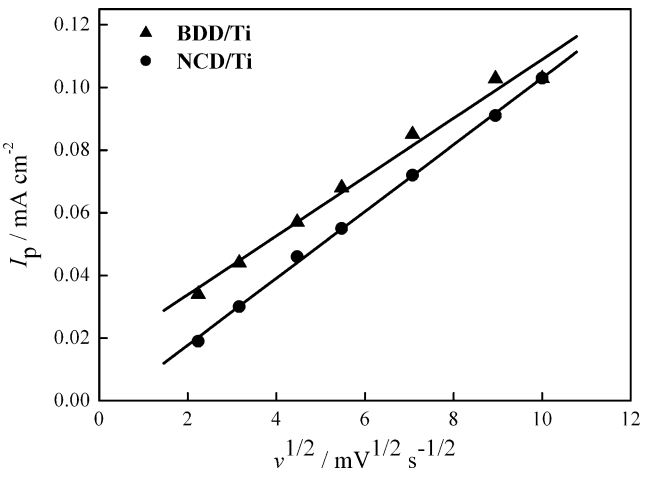

Fig. 7 Plots of I_p versus $v^{1/2}$ for the BDD/Ti and NCD/Ti electrodes obtained in 1.0 mmol L^{-1} $Fe(CN)_6^{4-/3-}$ + 1.0 mol L^{-1} KCl solution

intercept for BDD/Ti electrode, the linear behavior observed in the plot I_p as a function of $v^{1/2}$ may be considered as a kinetic parameter, also confirming the quasi-reversible electron transfer kinetic. Furthermore, it is also observed that I_p values are highest for the BDD/Ti electrode compared to those for NCD/Ti electrode. Two reasons may be attributed for these high I_p values, (1) increase of the high electrical conductivity due the boron doping presented in this film, which is responsible to the increase of crystallographic defects and (2) a more active surface for electron transfer reaction due to the smaller amount of sp^2 carbon impurities, which contribute to the presence of a low amount of oxygen terminated in the BDD surface.

The third aspect to be considered with respect to electrode kinetic is the surface roughness. According to SEM results (see Fig. 1), it is observed that the surface of NCD/Ti electrode is characterized by a drastic reduction of the grain sizes. This decrease in the grain size consequently decreases the surface roughness of NCD/Ti electrode. In this way, the surface of BDD/Ti electrode is rougher than that for NCD/Ti electrode. Such condition also reveals more rapid electron transfer kinetic for the BDD/Ti electrode. Similar results were shown by Pleskov et al. [30], which evaluated the electrochemical response of different BDD electrodes deposited on the Ti substrate and submitted to different treatment to obtain different roughness level. It was observed that electron transfer reactions are faster for the electrodes with greater surface roughness.

Taking into account the kinetics parameters evaluated for the $Fe(CN)_6^{4-/3-}$ redox couple, a strong influence of the surface conditions, associated to sp^2 carbon impurities amounts, active surface and surface roughness, was verified in the electron transfer kinetic on these electrodes. BDD/Ti and NCD/Ti electrodes showed a quasi-reversible behavior. However, the BDD/Ti electrode presented fastest electron transfer kinetic. The quasi-reversible behavior of redox reactions investigated with these electrodes may be associated with the low electron transfer kinetic on these electrodes are insufficient to keep the equilibrium of species in the solution interface.

Conclusions

In this paper, hybrid three-dimensional electrodes grown on porous Ti were produced. Two different electrodes are presented: BDD/Ti and NCD/Ti. From optimized parameters, by ourselves, we are able to produce Ti substrates totally covered by a uniform and continuous film. From a morphological perspective, the electrodes produced were systematically investigated. The results illustrate that kinetic parameters are strongly affected by the morphologic

properties from both electrodes. The evolution of the results as a function of kinetic parameters was accomplished by carrying out Raman spectroscopy measurements and SEM. The presence of sp^2 carbon impurities and surface roughness as well as the active surface area seems to be the major contributions to justify the kinetic parameters. These results were confirmed from voltammetric response of the BDD/Ti and NCD/Ti electrodes using $Fe(CN)_6^{4-/3-}$ redox couple. The different surface conditions mentioned above provided different votammetric behaviors resulting to peaks not well-defined for the $Fe(CN)_6^{4-/3-}$ redox process. Using these results, we have shown that the knowledge of film morphology is crucial to analyze the results from cyclic voltammograms.

Acknowledgements We are so grateful to FAPESP (process nos. 2008/04968-1 and 2007/00013-4) and CNPq (process no. 141966/2005-0, 471356/2006-9, and 555029/2005-6) for financial support.

References

1. Braga NA, Cairo CAA, Almeida EC, Baldan MR, Ferreira NG (2008) Diam Relat Mater 17:1891. doi:10.1016/j.diamond.2008.04.002
2. Braga NA, Cairo CAA, Almeida EC, Baldan MR, Ferreira NG (2009) in press
3. Cappuccio G, Sessa V, Terranova ML (1996) Appl Phys Lett 69:4176. doi:10.1063/1.116977
4. Swain GM (1994) J Electrochem Soc 141:3382. doi:10.1149/1.2059343
5. Vinokur N, Miller B, Avyigal Y, Kalish R (1996) J Electrochem Soc 143:L238. doi:10.1149/1.1837157
6. Pleskov YV, Sakharova AY, Krotova MD, Bouilov LL, Spitsyn BV (1987) J Electroanal Chem 228:19. doi:10.1016/0022-0728(87)80093-1
7. Szunerits S, Boukherroub R (2008) J Solid State Electrochem 12:1205. doi:10.1007/s10008-007-0473-3
8. Kondo T, Niwano Y, Tamura A, Ivandini TA, Einaga Y, Tryk DA, Fujishima A, Kawai T (2008) Electroanalysis 20:1556. doi:10.1002/elan.200804212
9. Denisova AE, Pleskov YV (2008) Russ J Electrochem 44:1083. doi:10.1134/S1023193508090152
10. Chuanuwatanakul S, Chalapakul O, Motomizu S (2008) Anal Sci 24:493. doi:10.2116/analsci.24.493
11. Swain GM (1994) Adv Mater 6:388. doi:10.1002/adma.19940060511
12. Chen Q, Granger MC, Lister TE, Swain GM (1997) J Electrochem Soc 144:3806. doi:10.1149/1.1838096
13. Declements R, Hirsche BL, Granger MC, Xu J, Swain GM (1996) J Electrochem Soc 143:L150. doi:10.1149/1.1836958
14. Declements R, Swain GM (1997) J Electrochem Soc 144:856. doi:10.1149/1.1837500
15. Zhu JZ, Yang SZ, Xu CF, Fan HZ (1995) Frenesius' J Anal Chem 352:389. doi:10.1007/BF00322239
16. Duo I, Michaud PA, Haenni W, Perret A, Comninellis CH (2000) Electrochem Solid-State Lett 3:325. doi:10.1149/1.1391137
17. Javier Del Campo F, Goeting CH, Morris D, Foord JS, Neudeck A, Compton RG, Marken F (2000) Electrochem Solid-State Lett 3:224. doi:10.1149/1.1391008
18. Wang J, Swain GM, Tachibana T, Kobashi K (2000) Electrochem Solid-State Lett 3:286. doi:10.1149/1.1391126
19. Popa E, Kubota Y, Tryk DA, Fujishima A (2000) Anal Chem 72:1724. doi:10.1021/ac990862m
20. Koppang MD, Witek M, Blau J, Swain GM (1999) Anal Chem 71:1188. doi:10.1021/ac980697v
21. Manivannan A, Tryk DA, Fujishima A (1999) Electrochem Solid-State Lett 2:455. doi:10.1149/1.1390869
22. Peiling Z, Jianzhong Z, Shenzhong Y, Xikang Z, Guoxiong Z (1995) Fresenius' J Anal Chem 353:171. doi:10.1007/BF00322953
23. Honda K, Rao TN, Tryk DA, Fujishima A, Watanabe M, Yasui K, Masuda H (2000) J Electrochem Soc 147:659. doi:10.1149/1.1393249
24. Rao TN, Fujishima A (2000) Diam Relat Mater 9:384. doi:10.1016/S0925-9635(99)00234-4
25. Niu C, Sichel EK, Hoch R, Moy D, Tennent H (1997) Appl Phys Lett 70:1480. doi:10.1063/1.118568
26. Tanahashi I, Yashida A, Nishino A (1990) J Electrochem Soc 137:3052. doi:10.1149/1.2086158
27. Ryan G, Pandit A, Apatsidis DP (2006) Biomaterials 27:2651. doi:10.1016/j.biomaterials.2005.12.002
28. Setoyama D, Matsunaga J, Muta H, Uno M, Yamanaka S (2004) J Alloys Compd 358:156. doi:10.1016/j.jallcom.2004.04.132
29. Senkov ON, Chakoumakos BC, Jonas JJ, Froes FH (2001) Mater Res Bull 36:1431. doi:10.1016/S0025-5408(01)00604-3
30. Pleskov YV, Evstefeeva YE, Krotova MD, Py L, Shih HC, Varnin VP, Teremetskaya IG, Vlasov II, Ralchenko VG (2005) J Appl Electrochem 35:857. doi:10.1007/s10800-005-2572-0
31. Gerger I, Haubner R, Kronberger H, Fafilek G (2004) Diam Relat Mater 13:1062. doi:10.1016/j.diamond.2004.01.025
32. Chen X, Chen G (2004) J Electrochem Soc 151:B214. doi:10.1149/1.1651529
33. Braga NA, Cairo CAA, Ferreira NG (2007) Quim Nova 30:450
34. Ferreira NG, Silva LLG, Corat EJ, Trava Airoldi VJ, Iha K (1999) Braz J Phys 29:760
35. Haubner R, Lux B (2002) Int J Refract Met Hard Mater 20:93. doi:10.1016/S0263-4368(02)00006-9
36. Bühlmann S, Blank E, Haubner R, Lux B (1999) Diam Relat Mater 8:194. doi:10.1016/S0925-9635(98)00258-1
37. Askari SJ, Akhtar F, Chen GC, He Q, Wang FY, Meng XM et al (2007) Mater Lett 61:2139. doi:10.1016/j.matlet.2006.08.033
38. Fu YQ, Yan BB, Loh NL, Sun CQ, Hing P (1999) J Mater Sci 34:2269. doi:10.1023/A:1004569406535
39. May PW, Mankelevich YA (2008) J Phys Chem C 112:12432. doi:10.1021/jp803735a
40. Knight DS, White WB (1989) J Mater Res 4:385. doi:10.1557/JMR.1989.0385
41. Chu PK, Li L (2006) Mater Chem Phys 96:253. doi:10.1016/j.matchemphys.2005.07.048
42. Ferrari AC, Robertson J (2001) Phys Rev B 64:075414. doi:10.1103/PhysRevB.64.075414
43. Silva LLG, Corat EJ, Barros RCM, Trava-Airoldi VJ, Leite NF (1999) Mater Res 2:1
44. Zhang RJ, Lee ST, Lam YW (1996) Diam Relat Mater 5:1288. doi:10.1016/0925-9635(96)00539-0
45. Colineau E, Gheeraert E, Deneuville A, Manbou J, Brunet F (1997) Diam Relat Mater 6:778. doi:10.1016/S0925-9635(96)00705-4
46. Woehrl N, Buck V (2007) Diam Relat Mater 16:748. doi:10.1016/j.diamond.2006.11.059
47. Cicala G, Bruno P, Benedic F, Silva F, Hassouni K, Senesi GS (2005) Diam Relat Mater 14:421. doi:10.1016/j.diamond.2004.12.025
48. Martin HB, Argoitia A, Landau U, Anderson AB, Angus JC (1996) J Electrochem Soc 6:L133. doi:10.1149/1.1836901

49. Granger MC, Xu JS, Strojek JW, Swain JM (1999) Anal Chim Acta 397:145. doi:10.1016/S0003-2670(99)00400-6
50. Show Y, Witek MA, Sonthalia P, Swain GM (2003) Chem Mater 15:879. doi:10.1021/cm020927t
51. Panizza M, Cerisola G (2005) Electrochim Acta 51:191. doi:10.1016/j.electacta.2005.04.023
52. Foti G, Gandini D, Comninellis C, Perret A, Haenni W (1999) Electrochem Solid-State Lett 5:228. doi:10.1149/1.1390792
53. Granger MC, Swain GMJ (1999) J Electrochem Soc 146:4551. doi:10.1149/1.1392673
54. Tryk DA, Tsunozaki K, Rao TN, Fujishima A (2001) Diam Relat Mater 10:1804. doi:10.1016/S0925-9635(01)00453-8
55. Greef R, Peat R, Peter LM, Pletcher D, Robinson J (1985) Instrumental methods in electrochemistry. Wiley, New York
56. Chen P, McCreey RL (1996) Anal Chem 68:3958. doi:10.1021/ac960492r